Interface investigation in nanostructured BaTiO3/silica composite ceramics

U-Chan Chung Seu, Catherine Elissalde, Frédéric Mompiou, Jérôme Majimel, Sonia Gomez, Claude Estournès, Sylvain Marinel, Andréas Klein, François Weill, Dominique Michau, et al.

Interface Investigation in Nanostructured $BaTiO_3$/Silica Composite Ceramics

U-Chan Chung,[‡] Catherine Elissalde,[†,‡] Frédéric Mompiou,[§] Jérôme Majimel,[‡] Sonia Gomez,[‡] Claude Estournès,[¶] Sylvain Marinel,[‖] Andreas Klein,[**] François Weill,[‡] Dominique Michau,[‡] Stéphane Mornet,[‡] and Mario Maglione[‡]

[‡]CNRS, Université Bordeaux, ICMCB, F-33608 Pessac Cedex, France

[§]CEMES-CNRS, BP 93347, 31055 Toulouse Cedex 4, France

[¶]CIRIMAT et Plateforme Nationale CNRS de Frittage Flash, PNF2 MHT, Université Paul Sabatier, 33062 Toulouse, France

[‖]CRISMAT, UMR 6508 CNRS, 14050 Caen Cedex 4, France

[**]Darmstadt University of Technology, Institute of Materials Science, Surface Science Division, Petersenstrasse 23, 64287 Darmstadt, Germany

Silica-coated ferroelectric particles are promising building blocks for functional bulk composites such as dielectric resonators, supercapacitors, or multiferroics. The ferroelectric/silica interface was fully investigated by means of high-temperature *in situ* X-ray diffraction, high-resolution scanning electron microscopy, and X-ray photoelectron spectroscopy. Mechanisms occurring at the interface were visualized using high-resolution postmortem and *in situ* transmission electron microscopy performed at different temperatures. On the light of this interface investigation, we have used advanced sintering processes such as spark plasma sintering and microwave sintering to obtain nanostructured composite ceramics and to evaluate their dielectric properties.

I. Introduction

The coating of oxide or metallic particles by a continuous silica shell (core–shell architecture) has led to significant advances in functional materials, thus increasing drastically the range of applications (photonic crystals, luminescent semiconductors, biomedical magnetic systems, etc.).[1,2] As high-temperature processes are not required to obtain the macroscopic composite, the initial nanoscale design is preserved. Property control is based on the periodicity and tunability of interparticle spacing (particle size, coating thickness) that drives the coupling between neighboring particles.[3–7]

However, in high-density materials such as nanostructured electroceramics, preserving the nanoscale architecture is yet to be achieved, mainly because of the high-temperature sintering step. Core–shell building blocks were already used to favor solid-state reaction at the nanoscale, in order to (i) tune dielectric properties, (ii) delay or enhance densification, (iii) avoid grain growth during sintering, and (iv) improve the mechanical properties of sintered nanoparticles.[8–14] In these dense 3D bulk materials, macroscopic properties are intimately resulting from the thermal treatment. Studies devoted to $BaTiO_3$ (BT)–silica (SiO_2)-based composites provide an illustration of the drastic role of temperature and of the initial composite architecture.[15–18]

Other critical issues are the specific role and composition of the core–shell interface.

Fresnoite, $Ba_2TiSi_2O_8$, clearly identified as a secondary phase growing inbetween the two components, is described in the literature as a ferroelectric material with dielectric, pyroelectric, and piezoelectric properties.[19,20] None of the previous reports referring to BT/SiO_2 ceramics were focused on a specific study of the interface; silica is mainly used as an additive for lowering the sintering temperature.[21,22] The full investigation of interfaces in such composites strongly depends on the complex control of interfaces, including the design of the starting composite. There is an obvious interest in understanding, and thus monitoring, such an intrinsically functional interphase formation, as the final properties and the possibility of additional functionalities will strongly depend on its nature (i.e., amorphous, partially, or completely transformed into crystalline fresnoite). Attaining such a level of interface control is of great interest for property tunability in the large area of functional electroceramics (dielectric resonators, tunable capacitors, antennas, supercapacitors, etc.).

Here, we propose a deep investigation of the BT/SiO_2 interface, down to the atomic resolution, using techniques such as *in situ* transmission electron microscopy (TEM), postmortem high-resolution transmission electron microscopy (HRTEM), and X-ray photoelectron spectroscopy (XPS). Core–shell particle design, BT@SiO_2, was chosen as initial building block of the ceramic composites because the full coverage of each particle is definitely a prerequisite for the control of the chemical and structural mismatch between the core and shell, at the grain scale. Such a coating quality is also mandatory to uniformly transfer the property modification from the grain scale to the 3D dense ceramic. As previously reported,[9] the soft chemistry route we used for BT@SiO_2 enables a uniform, continuous, and homogeneous nanoscale coating of each individual ferroelectric particle. An additional advantage of ferroelectric@silica architecture is that silica enables additional functionality of the ferroelectric component, by ways of surface modification: this way, either the coexistence of ferroelectricity and ferromagnetism or low loss supercapacitor were obtained.[23,24]

M. Menon—contributing editor

This work was financially supported by the French National Center for Scientific Research (CNRS), the National Research Agency (ANR), and the European Community in the frame of the "FAME" network of excellence.

[†]Author to whom correspondence should be addressed. e-mail: elissald@icmcb-bordeaux.cnrs.fr

II. Experimental Procedure

(1) Synthesis and Standard Sintering of BT@SiO_2 Particles

Barium titanate particles of mean diameter 300 and 500 nm (BT500) were purchased from Sakai Chemical Co. (Fukushima, Japan). All the particles had been individually coated with a homogeneous amorphous silica shell of 5-nm-thickness (Si5) using a method derived from the so-called Stöber process. The surface of the BT particles had to be activated by acidic treatment with nitric (1*M*) and citric (0.01*M*) acids before silica coating. The reaction occurred in a water/alcohol/ammonia solution using tetraethoxysilane as the silica source. The procedure is described in details elsewhere.[9]

Standard sintering was performed on BT500–Si5 powder at 800°, 1000°, and 1210°C during 3 h with two additional steps at 250° and 600°C of 1 h each, under oxygen atmosphere and with a heating rate of 100°C/h.

(2) Characterization of the BT/SiO_2 Interface

Temperature-dependent X-ray diffraction (XRD) has been performed using a Philips X'Pert automatic diffractometer (Philips, Almelo, the Netherlands) (Cu$K\alpha$ radiation) equipped with a variable-temperature Anton Paar HTK16 Pt stage. The temperature of the sample has been increased from room temperature up to 1205°C at a heating rate of 5°C/min and the patterns have been recorded at 15°C intervals in the range $15° \leq 2\theta \leq 60°$ with a step size of 0.02°, counting two seconds per step.

The microstructural characterization of the sintered compacts was performed using a scanning electron microscope (SEM) JEOL JSM 6360A (JEOL, Cruissy-sur-Seine, France) and a high-resolution scanning electron microscope (HRSEM) JEOL 6700F. A thin Au/Pd coating was deposited on the ceramics fracture surface before observation.

TEM *in situ* heating experiments were carried out in a JEOL 2010 operated at 200 kV using a Gatan high-temperature TEM holder (Gatan, Evry, France) and SPI silicon nitride membrane window grids. Temperature was controlled by a thermocouple with an accuracy of a few degrees. The dynamical response under thermal solicitation was monitored by means of DVD/HD recording using a MEGAVIEW II CCD camera.

STEM-EDX and HRTEM observations were performed using a JEOL 2200 FS equipped with a field emission gun, oper-

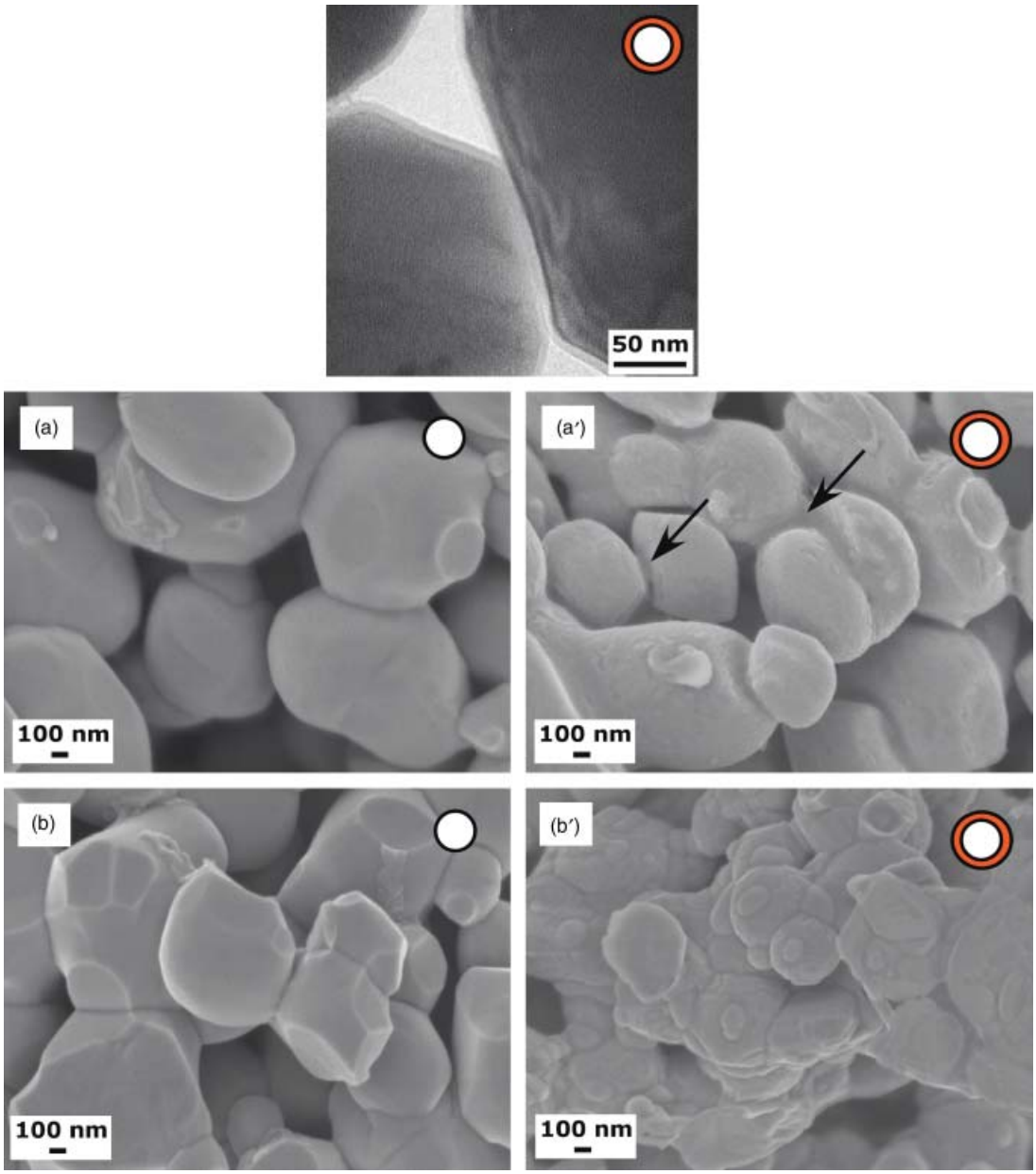

Fig. 1. Top: Transmission electron microscopy image of silica (5 nm)-coated BT (500 nm) (BT500–Si5) particles. High-resolution scanning electron microscope fracture images of uncoated BT (500 nm) ceramics and BT500–Si5 sintered at 800°C (a, a′), 1000°C (b, b′). (a′) Arrows indicate neck formation.

ating at 200 kV and with a point resolution of 0.19 nm. HRTEM images were recorded using a Gatan Ultrascan CCD 2 k × 2 k and Digital Diffractograms were calculated using the Gatan Digital Micrograph® software.

XPS experiments were performed using an ESCALAB 220i XL spectrometer with monochromatic Al$K\alpha$ excitation. Sample charging was partially compensated by an electron flood gun. $BaCO_3$, TiO_2, and SiO_2 were used as precursors for the preparation of fresnoite powder via a solid-state reaction. Fresnoite ceramics were obtained by conventional sintering at 1350°C during 3 h. The BT thin films were processed using standard radio frequency sputtering deposition on amorphous SiO_2 substrates.

(3) Advanced Sintering Processes and Dielectric Measurements

The BT(500 nm)–SiO_2 (5 nm) powders were sintered using spark plasma sintering (SPS) equipment (Dr Sinter SPS-2080 SPS Syntex INC Japan of the Plateforme Nationale de Frittage Flash (PNF2) of CNRS located at Toulouse, France). Core–shell powders (without any sintering aids) were loaded into a cylindrical die of 8 mm inner diameter. The pulse sequence was 12-2 (pulses—dead time or zero current). The temperature was raised to 600°C over a period of 3 min, and from this point it was monitored and regulated by an optical pyrometer focused on a small hole located at the surface of the die. A heating rate of 100°C/min was used to attain the final temperature of 1050°C under an argon (Ar) atmosphere. SPS experiments were performed under a uniaxial pressure of 50 MPa. To observe the microstructure of the SPS ceramics, thin slices were obtained using an ''ultracut S'' ultramicrotome. The ceramic has been clamped directly in the microtome sample holder and a diamond knife has been used to obtain slices of 65-nm-thickness; the slices were then deposited on a copper grid.

Microwave sintering experiments were performed in a TE102 rectangular microwave cavity. The details of the microwave device have been described in a previous paper.[25] A cylindrical $LaCrO_3$ susceptor was used and placed perpendicular to the electrical field component. The samples used for microwave sintering were thermally pretreated at 250° and 600°C for 1 h with a heating rate of 100°C/h. As in standard sintering conditions, these two additional annealing steps were performed to ensure removal impurities resulting from the soft chemistry route used.

Then, the preheated disk was placed in an alumina crucible and positioned in the middle of the cylindrical susceptor. The incident power was fixed at 600 W and the thermal cycle duration was 5 min. The sample is, hence, quenched in order to freeze the high-temperature microstructure.

The permittivity and dielectric losses of the ceramics were recorded as a function of temperature (300–500 K) and frequency (100 Hz–100 kHz) using a Wayne–Kerr component analyzer 6425. Dielectric measurements were performed on the ceramic discs (diameter 6 mm, thickness 1 mm) with gold electrodes sputtered on the circular faces.

III. Results and Discussion

(1) Microstructural Investigations of Sintered BT@SiO_2 Particles

Calcinations were firstly performed at different temperatures on pellets made of core–shell BT (500 nm)–SiO_2 (5 nm) particles (denoted as [BT500–Si5]) in order to gradually probe the effect of temperature on the interface modification between barium titanate and the initially coated amorphous silica nanolayer. Such a step-by-step approach was performed on both coated and uncoated BT particles. HRSEM pictures of BT500–Si5 calcinated at 800°C showed the formation of interparticle necks growth by a viscous flow (zones pointed by arrows in Fig. 1(a′)).[26,27] The absence of shrinkage on the dilatometric curve and the density value similar to that of the green body (56%) support a nondensifying mass transport mechanism. The surface of the grains is rough, and an ''orange skin'' aspect on some grains is observed resulting from the dehydration (removal of physically adsorbed water) and deshydroxylation processes involving condensation of the surface silanol groups.[28,29] When the sintering temperature is raised up to 1000°C, a drastic change occurs in the microstructure. The formation of blisters on the surface of the coated grains is clearly observed whereas uniform and glossy grain surfaces appear on the uncoated sample calcinated at 1000°C in the same conditions (Figs. 1(b) and (b′)). The density remains lower than 90% when the coated powder is sintered at 1210°C and grain growth is much more pronounced in the case of the ceramic made of uncoated grains. *In situ* XRD as a function of temperature was performed to accurately probe the on-set of the fresnoite formation at the BT/SiO_2 interface and its thermal evolution. The fresnoite, $Ba_2TiSi_2O_8$, occurs on the XRD diagram recorded at 860°C and no titanium-rich phases such as $Ba_6Ti_{17}O_{40}$ were detected (Fig. 2(a)). The peculiar microstructure obtained at 1000°C can, thus, be correlated to fresnoite crystallization.

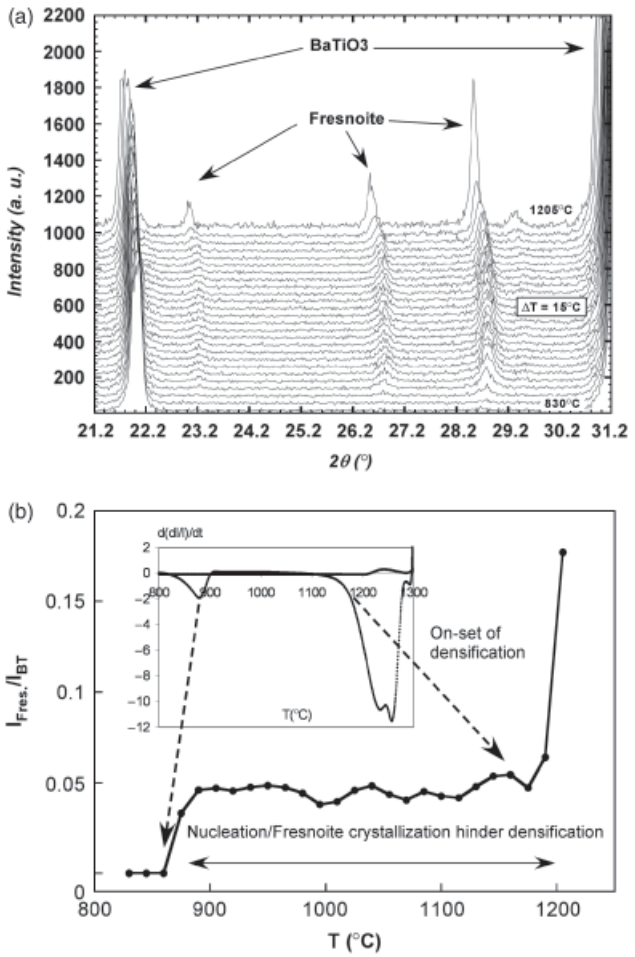

Fig. 2. (a) Temperature-dependent X-ray diffraction for temperatures ranging from 830°C up to 1205°C for BT500–Si5 powders. Fresnoite ($Ba_2TiSi_2O_8$) peaks clearly appear at 860°C. (b) Relative intensities between the fresnoite and the BT peaks, $I_{fresn.}/I_{BT}$ from *in situ* XRD as a function of temperature. Inset: Shrinkage rates as a function of temperature for BT500–Si5. Three regimes can be evidenced: 1, fast nucleation of fresnoite up to 900°C; 2, stabilization of $I_{fresn.}$/BT corresponding to hindered densification (plateau in the shrinkage rate) between 900 and about 1150°C; and 3, abrupt increase in the $I_{fresn.}/I_{BT}$ ratio signing to the onset of densification at temperatures higher than 1150°C.

(2) Discussion on the Mechanism of Fresnoite Formation

The surface of the BT grains is considered here to provide a site for heterogeneous nucleation of fresnoite crystals. This surface,

cleaned by an acidic treatment performed before the coating, is rich in barium vacancies, which can enhance diffusion fluxes. It is known for a long time that the Ba of BT surface dissolves at low pH and acts as a potential-determining ion (PDI) in the solution. This explains the difficulty to disperse BT particles in water.[30–32] In previous zeta potential studies, we observed that cleaning the particles with acidic treatment allowed removing these PDI from the surface of $Ba_{0.6}Sr_{0.4}TiO_3$ particles.[9] After HNO_3 treatment, the isoelectric point of these particles was shifted from 8.5 to 5.1, closer to the value of TiO_2 (5.5) and $SrTiO_3$ (5.1).[33] The onset of fresnoite nucleation was clearly determined at 860°C by XRD and thermal analysis. The evolution of the fresnoite formation as a function of temperature, was estimated considering the relative intensities between BT and the fresnoite main peaks ($I_{fresn.}/I_{BT}$) from *in situ* XRD experiments. Close correspondence with the dilatometric investigation carried on BT500–Si5 (shrinkage rate shown in insert) can be evidenced, allowing thus to propose a mechanism for the fresnoite formation and interface evolution (Fig. 2(b)). The increase of $I_{fresn.}/I_{BT}$ ratio in the range 800°–900°C obviously coincides to the first nucleation of fresnoite crystals. This is consistent with the first shrinkage observed in the same temperature range and which does not occur when BT and SiO_2 are sintered separately (not shown). Considering the initial continuous silica coating on each individual particle, we assume here that the fresnoite is formed uniformly and at the interface at the grain scale. A stabilization of the ratio $I_{fresn.}/I_{BT}$ is observed in exactly the same temperature range (900°–1150°C) as the plateau of the shrinkage rate. The formation of fresnoite crystallites hinders densification. Note that in the case of pure SiO_2 particles, densification starts at a temperature as low as 1050°C. The increase of the volume fraction of fresnoite inclusions, or the fresnoite particle growth, delays sintering by a viscous flow. However, at least up to 1000°C, these inclusions are not considered as rigid inclusions in view of the presence of amorphous silica, which contribute to lubricate the contact between them. The further increase in the

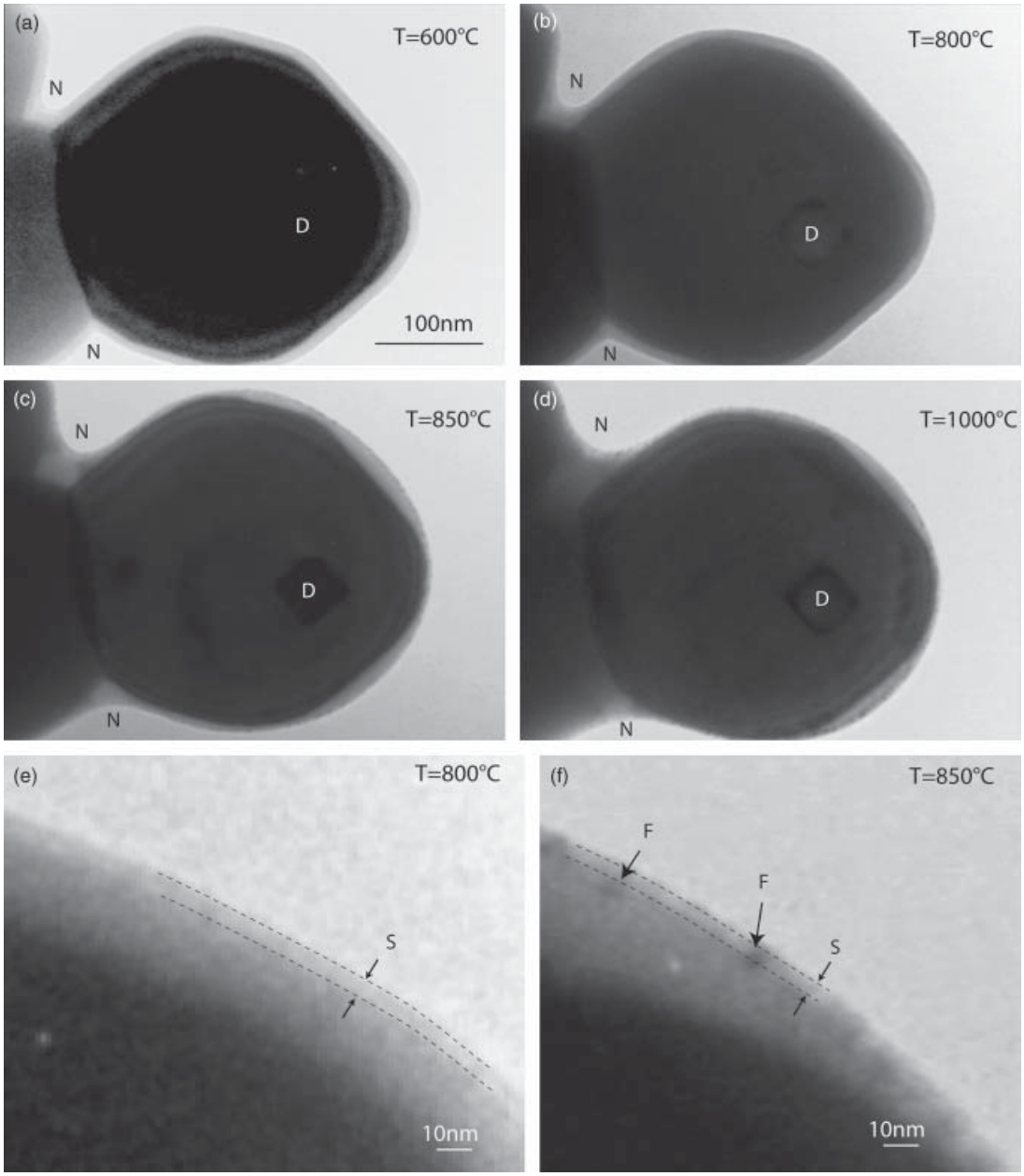

Fig. 3. Transmission electron microscopic micrographs of a core–shell particle taken during *in situ* heating experiment. Note the presence of surface defects (D) before the heating run. Below 850°C (a–b), viscous flow of silica softens necks between neighbouring particles (N). At 850°C (c), crystallites nucleate in the outer shell. The core–shell structure is, however, preserved up to 1000°C (d). Note that the necks tend to be smoother. (e) and (f) show the particle at a higher magnification, highlighting the crystallization formation (F) at 850°C in the outer shell (S). The silica shell (S) is indicated by arrows and delimited by dashed lines. The brightness rapidly decreasing from the outer shell to the particle center, is due to the sharp edges.

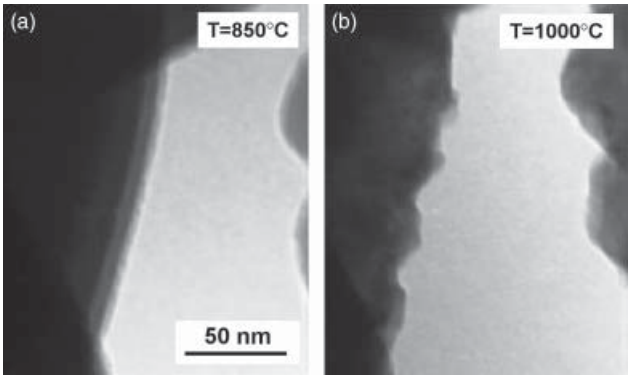

Fig. 4. Transmission electron microscopic micrographs taken during *in situ* heating experiment. Between 850°C (a) and 1000°C (b), a strong roughening of the surface occurs, leading to the formation of blisters.

$I_{fresn.}/I_{BT}$ ratio corresponds to the densification on-set at 1150°C. At this stage, the amorphous silica layer is practically fully consumed and transformed into fresnoite at the interface. It is difficult to conclude on the sintering mechanism between densifying viscous flow regime (a thin wetting silica layer with appropriate viscosity can be sufficient) and change into volume diffusion or grain boundary diffusion. Isothermal sintering performed at 1210°C did not provide a better insight into the sintering mechanism, suggesting that a combination of the two mechanisms occurs.

(3) In Situ TEM Experiments

To support the above-mentioned sintering model, *in situ* heating TEM experiments were performed up to 1000°C in order to visualize the gradual nanoscale transformation of fresnoite at the BT/SiO_2 interface. The aim was to obtain a direct imaging of the dynamics of the core–shell grains under thermal stress, i.e. the crystallization process at the interface. Initial 300-nm BT cores coated with 5-nm silica were used for imaging scale convenience. It was previously demonstrated that the interface evolution between silica and BT is not dependent on the ferroelectric core size.

Figures 3 and 4 show pictures extracted from a video sequence taken at different temperatures. Every picture was recorded after holding the set temperature for a few minutes. Every temperature step was achieved in less than a minute. In Fig. 3(a), a single core–shell particle of 300 nm in diameter is shown at 600°C. Because the particle is seen in projection, the silica shell (labeled S) appears as a thin 5-nm layer in the outer part of the particle (note the dashed line delimiting the shell in Figs. 3(e) and (f)). The absence of thickness fringes in the grain core but close to the boundary indicates that the particle is faceted (Fig. 3(a)). This implies the presence of sharp edges, which show an increase of brightness from the center, opaque to the electrons, to the thin outer shell. The same particle morphology is also seen in Fig. 6. Other particles with the same morphology are visible on the left part of the image (Fig. 3). In the areas labeled N, where grains are in contact, different grain surfaces can be easily distinguished. Electron diffraction indicates that the particles are single crystalline, but some small unidentified surface defects (marked D in Figs. 3(a)–(d)) are usually observed. Below 850°C, the silica shell does not exhibit any visible structural modifications (Figs. 3(b) and (e)). The observation of necks in the contact area seems to indicate that a viscous flow of silica has led to the formation of bridges between adjacent grains. This has also led to a global redistribution of matter around the core; one can see by comparing the particle shape in Figs. 3(a) and (d) that the shell surface is less faceted at higher temperature. At 850°C, some crystallites, already as large as the silica-shell thickness, are visible everywhere in the outer shell (Figs. 3(c) and (f)). They appear as black dots in the silica amorphous shell. This strongly suggests that they should correspond to the fresnoite, as observed during XRD experiments. Such a good agreement with XRD data shows that both e-beam irradiation and vacuum have negligible influence on sintering and crystallization processes. Only a possible electron beam heating and charging effects have to be considered. Silica bridges in the necked regions keep growing due to the combination of capillarity forces and a faster diffusion at higher temperature. This confirms that fresnoite crystallites do not act as pinning centers preventing the viscous flow at least up to 1000°C. Despite the existence of fresnoite crystallites that should consume the silica, the amorphous shell is still preserved up to 1000°C (Figs. 3(c) and (d)). From 850° up to 1000°C, the surface roughness increases as depicted in Fig. 4, which shows pictures taken in another area. In some other particles observed, this roughening leads to the formation of blisters such as seen on HRSEM pictures (see Fig. 1(b′)). Experiments carried out at different temperatures seem to indicate that this roughening is thermally activated.

(4) STEM-EDX and HRTEM Experiments

To supplement this investigation with chemical probing at the nanoscale, STEM-EDX analysis has been carried out postmortem on the sample investigated by *in situ* TEM at 1000°C as well as on the starting $BT@SiO_2$ material.

One can observe in Figs. 5(a) and (b) that as-prepared BT cores are homogeneously coated with an approximately 20 nm-

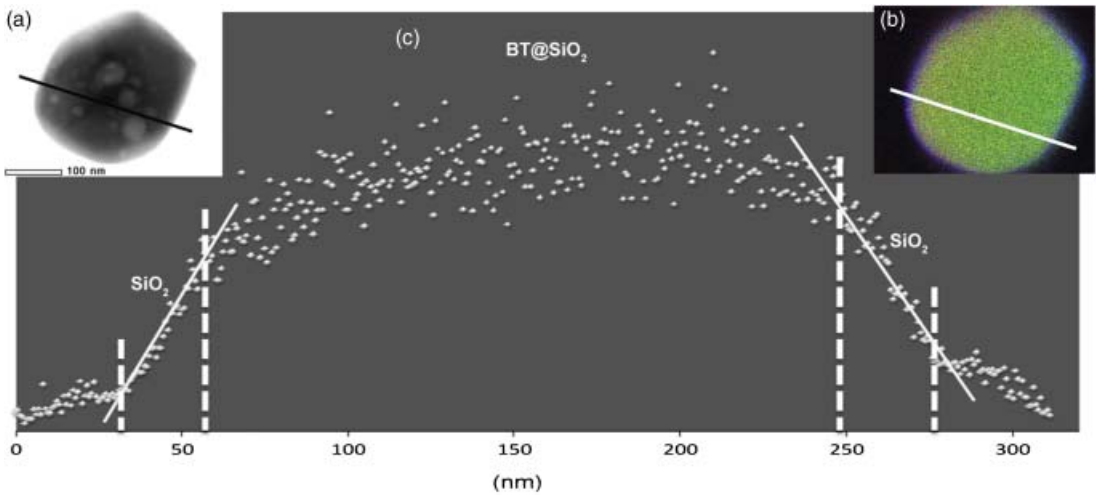

Fig. 5. (a) STEM micrograph of a $BaTiO_3$–silica starting particle. (b) Three colors image drawn from the EDX map of the particle presented on (a). The red, green, and blue colors correspond to the oxygen, the barium, and the silicon elements, respectively. (c)[Ba]/[Si] profile plotted from (b) the map along the black line of figure (a). Dashed lines indicate the frontiers between the inner BT core and the outer silica shell.

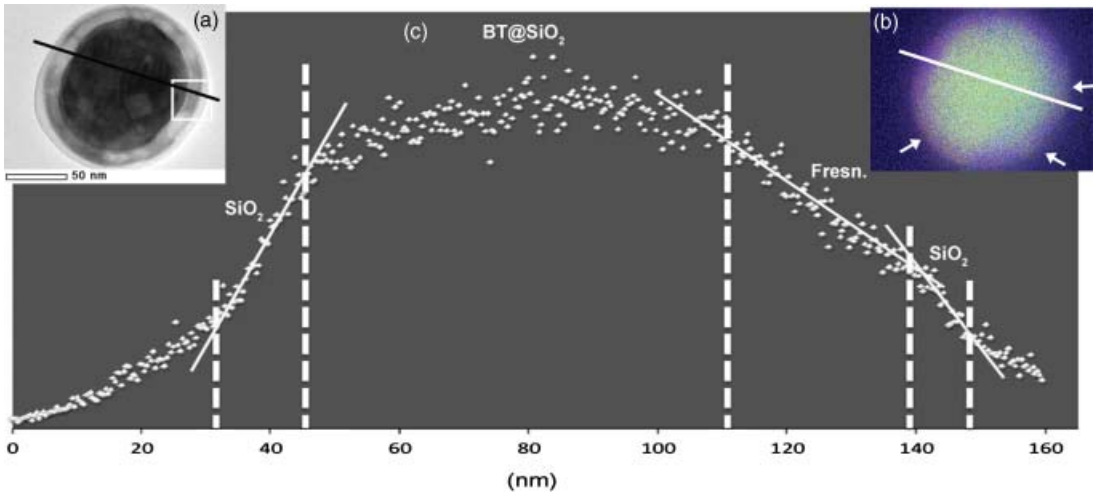

Fig. 6. (a) STEM micrograph of a particle of the $BaTiO_3$–silica sample investigated by *in situ* TEM at 1000°C. (b) Three colors image drawn from the EDX map of the particle presented on (a). The red, green, and blue colors correspond to the oxygen, the barium, and the silicium elements, respectively. Fresnoite clusters correspond to the zones marked by arrows. (c)[Ba]/[Si] profile plotted from (b) the map along the black line of figure (a). Dashed lines indicate the frontiers between the inner BT core, the fresnoite clusters, and the outer silica shell.

thick silica shell. Please note that the silica-shell thickness is slightly overvalued compared with the 5 nm mentioned previously. This can be due to the long-time exposure under the focused electron beam, which favors the growth of the outer silica shell because of its collisionnal and local heating effects. The slope of the [Ba]/[Si] profile (Fig. 5(c)) plotted from STEM-EDX

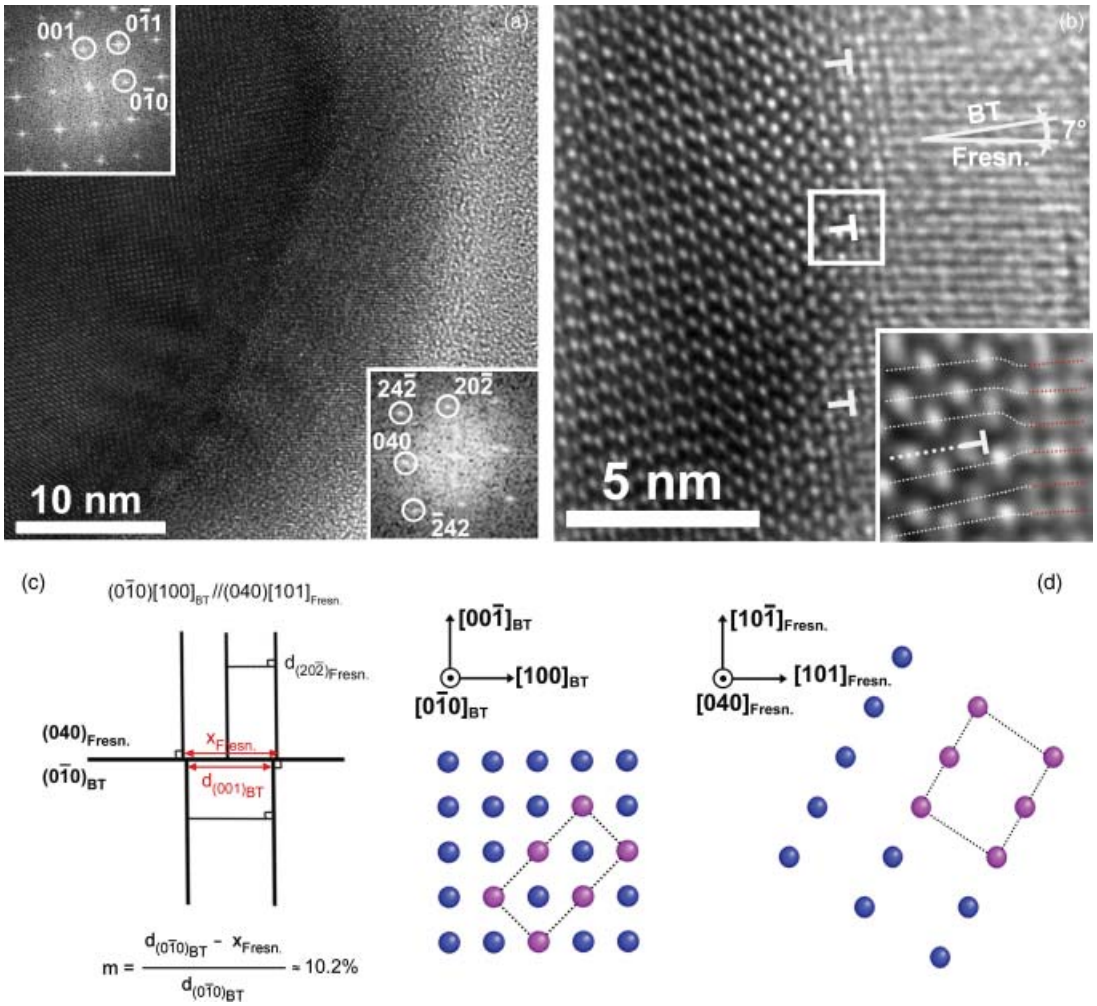

Fig. 7. (a) High-resolution transmission electron microscopy micrograph of a particle of $BaTiO_3$–silica investigated by *in situ* TEM at 1000°C. This image corresponds to the zone delimited by the white square on (a). On the upper left and lower right, insets shown are the indexed digital diffractograms of the BT core and of the fresnoite cluster, respectively. (b) Zoom on the interface zone between the BT core and the fresnoite cluster. White and red dashed lines represented on the inset correspond to BT and fresnoite reticular planes, respectively. The additional half-plane of the BT structure is a misfit dislocation represented by the $\perp$ symbol. (c) Schematic view of the BT/fresn. interface zone according to the $(0\bar{1}0)[100]_{BT}$// $(040)[101]_{fresn.}$ orientation relationship and calculated $\Delta a/a$ lattice misfit (m). (d) Projection of Ba atoms of BT and fresn. interface planes. Atoms highlighted in pink can face each other from both sides of the interface, the rectangles in dashed lines being distorted according to the misfit value.

map is rather flat for the inner core zone and decreases abruptly for the silica shell, confirming that BT particles are homogeneously coated and pointing out that the interface zone between the core and the shell is well defined.

The same experiment performed on the *in situ* sample shows a slightly thicker silica shell, highlighting its viscous character once the 1000°C range of temperature is attained. But the most important feature is the observation of dark-contrasted zones inside the silica shell (Fig. 6(a)). These zones pointed by arrows on the three color image of Fig. 6(b) and appearing pinker than the purple outer shell (larger amount of green color component), are revealed to be Ba enriched. Moreover, whereas the extreme left- and right hand-side slopes of the [Ba]/[Si] profile plotted in Fig. 6(c) are rather similar to those plotted in Fig. 5(c) for the starting material, it softens for the dark-contrasted zone.

One can see on the HRTEM micrograph in Figs. 7(a) and (b) that the dark-contrasted clusters are crystallized as reticular planes can be observed. The indexation of digital diffractograms and the measurement of reticular distances on HRTEM images unambiguously points toward fresnoite (space group *P4bm*, $a = 8.518(2)$ Å, $c = 5.211(1)$ Å)[ICDD-PDF: 22-0513]. This strongly suggests that the diffusion process occurring from the BT core (Ba diffusion into silica shell) led to the nucleation of fresnoite clusters into the silica shell. It is worth noting that edges or corners of the crystalline BT grains seem to be energetically favorable for fresnoite nucleation.

Furthermore, the crystallographic investigation of the interface between BT and fresnoite showed that fresnoite clusters grow at the surface of the BT cores according to the following orientation relationship (Fig. 7(c)):

$$(0\bar{1}0)[100]_{BT}//(040)[101]_{fresn.}$$

These $(0\bar{1}0)_{BT}$ and $(040)_{fresn.}$ interface planes are Ba rich. Moreover, similar tilted rectangular patterns (in pink in Fig. 8(d) can be found in the $(0\bar{1}0)_{BT}$ and $(040)_{fresn.}$ planes and belonging to the $(001)_{BT}$ and $(20\bar{2})_{fresn.}$ facing each other from both sides of the interface plane. The growth of fresnoite clusters on BT cores is then chemically and structurally favored.

As for other nanocomposite systems, one can also observe in Fig. 7(b), the presence of a dislocation network, perpendicular to the interface plane between the BT core and the fresnoite clusters.[34] It seems that the lattice mismatch between the two phases is relaxed by dislocation creation rather than elastic deformation. The Δa/a lattice misfit value of about 10.2%, is approximately in good agreement with the presence of three dislocations for 30 lattice plane, as we can see in Fig. 7(b) (Fig. 7(c)). Finally, note that the 7° angle between the $(001)_{BT}$ and $(20\bar{2})_{fresn.}$ corresponds to an angular deviation from the epitaxial relationships mentioned above. This deviation increases as the interface plane length decreases.

(5) XPS Experiment

In contrast to TEM, XPS probes a large area and thus provides information over a large amount of particles. XPS spectra of BT powder coated with a 5-nm-thick SiO_2 shell are shown in Fig. 8 in comparison with a sputter-deposited BT thin film and two fresnoite reference samples (ceramic and BT/SiO_2 thin film after heating to 1000°C). The as-prepared core–shell powder shows a strong SiO_2 emission at ~103.5 eV binding energy and a weak Ba 4*d* emission with a binding energy of the $4d_{5/2}$ component of ~89 eV, which can be attributed to BT. Heating the powder to 1000°C in air strongly decreases the SiO_2 intensity and increases the Ba 4*d* intensity. Two distinct Ba 4*d* components can be identified, which correspond to the BT and the fresnoite references. The fresnoite phase is identified by the binding energy difference and the intensity ratio of the Si 2*p* and Ba 4*d* emissions. Considering the different intensities, the XPS spectrum of the air-heated core–shell powder (1000°C) is consistent with a partial coverage of BT by fresnoite particles. This is consistent

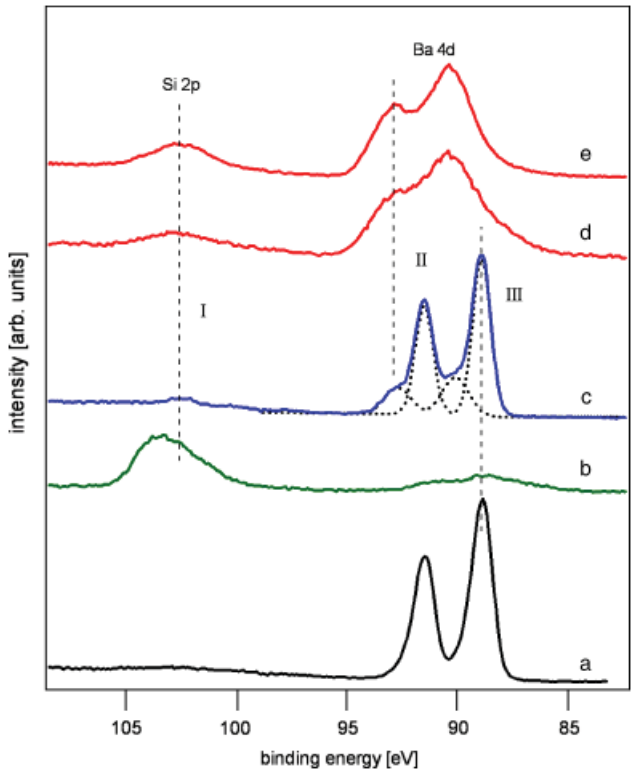

Fig. 8. X-ray photoelectron spectra of the Si 2*p*–Ba 4*d* region. Measured samples are (a) $BaTiO_3$ thin film on Pt, (b) $BaTiO_3$ powder covered with 5 nm of SiO_2, (c) sample (b) after heating to 1000°C in air, (d) $BaTiO_3$ thin film on SiO_2 after heating to 1000°C in air, which caused the transformation of the film to fresnoite, and (e) fresnoite ceramic. Component I corresponds to Si 2*p* in fresnoite, II to Ba $4d_{3/2}$ in fresnoite, and III to Ba $4d_{5/2}$ in $BaTiO_3$. Spectra are manually shifted in binding energy for a better identification of chemical species. The asymmetry observed for samples (b), (d), and (e) is attributed to inhomogeneous sample charging.

with postmortem and *in situ* TEM investigations. The close correspondence between the XPS spectra of the two fresnoite reference samples and the calcinated core–shell particles (c, d, e in Fig. 8) also indicates that XPS studies of thin-film samples can be useful for a detailed study of the interface chemistry between SiO_2 and BT. Thin-film samples might provide a considerable advantage compared with ceramic samples in such studies as they can be deposited onto conducting substrates. Thereby, charging effects, which often lead to considerable broadening and asymmetries of the core level lines, can be avoided.

To summarize all the previous microscopic investigations, interdiffusion between SiO_2 and BT leads to the formation of fresnoite which nucleates in the early stage of sintering, i.e. 860°C (*in situ* XRD). Even if cross diffusion at the BT/SiO_2 interface occurs, HRTEM confirmed the higher mobility and diffusion of Ba ions into the silica shell. The fresnoite crystallites occur preferentially at energetically and crystallographically favorable sites such as defects, vacancies, edges, corners, etc. As a result, the silica shell roughens (*in situ* TEM) and as confirmed by XPS, blisters are observed instead of homogeneous fresnoite coating. The dielectric measurements performed on composite ceramics are now described as intrinsic and extrinsic macroscopic probes.

(6) Advanced Sintering Processes and Dielectric Properties

The fresnoite $Ba_2TiSi_2O_8$ is described in literature as a new ferroelectric mineral exhibiting nearly constant permittivity values close to 10 between 300 and 600 K.[19,20] This second phase as well as the porosity decreases the permittivity in the composite compared with the uncoated BT but does not affect the Curie temperature of the BT core. As shown previously, a sintering

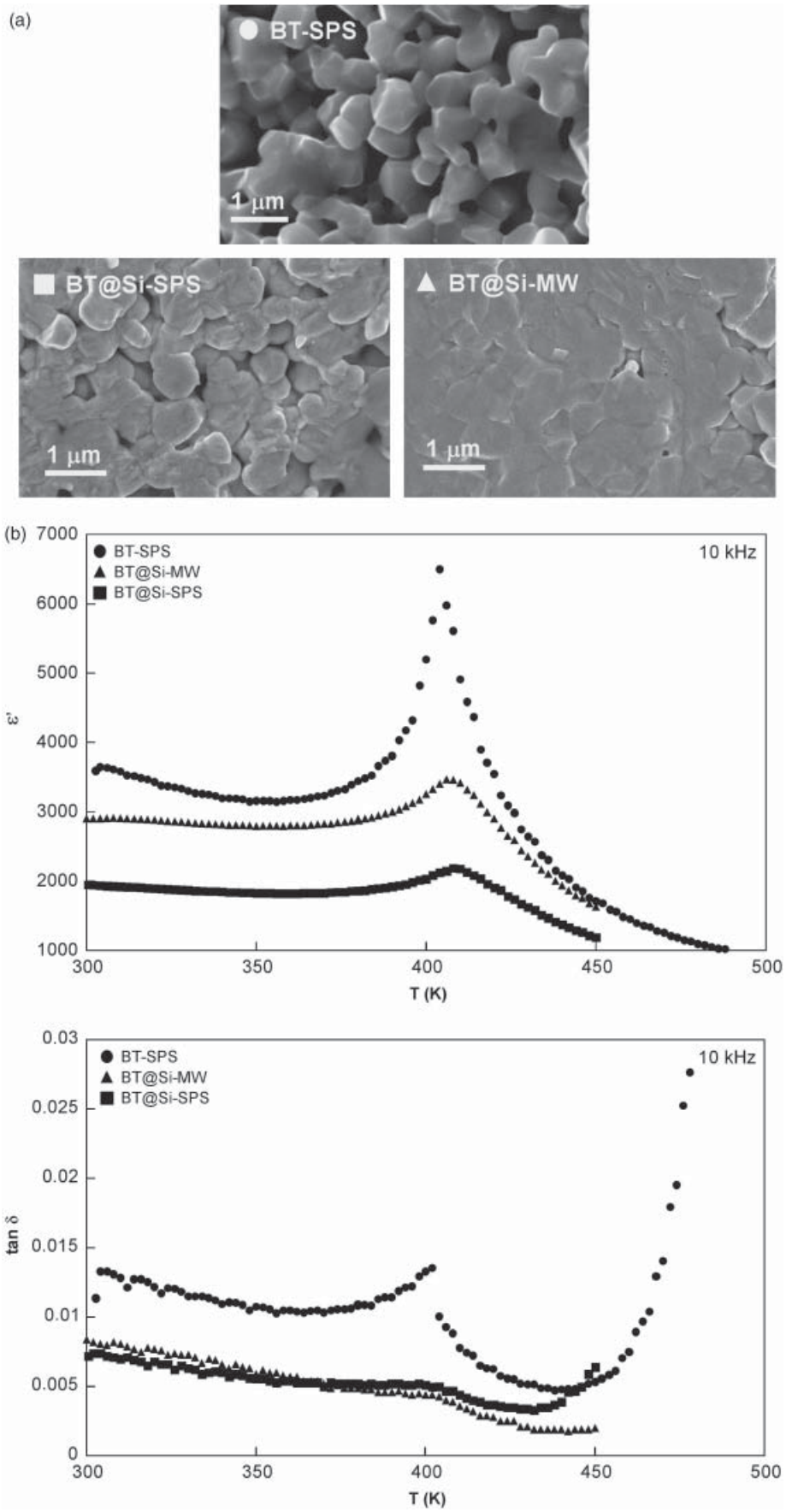

Fig. 9. (a) High-resolution scanning electron microscope microstructures and (b) the dielectric properties of uncoated BT500 ceramic sintered by SPS, BT500–Si5 sintered by spark plasma sintering (SPS) and microwave.

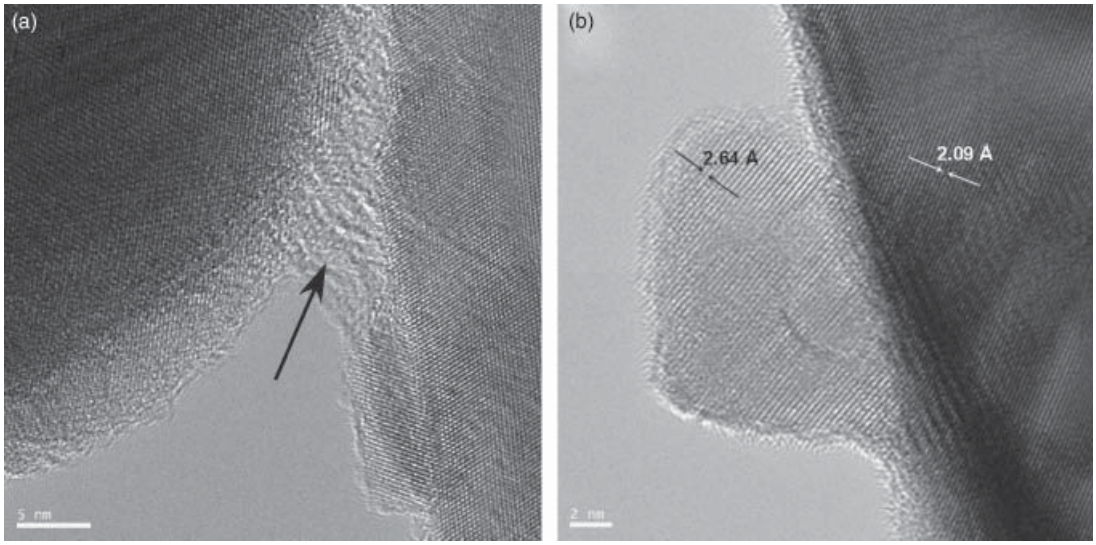

Fig. 10. (a) High-resolution transmission electron microscopy images of a 60-nm-thick slice obtained by ultramicrotomy of BT500–Si5 sintered at 1050°C by spark plasma sintering. (a) Arrow indicates an amorphous phase in the vicinity of the grain boundaries in between two crystallized grains. (b) Small crystal with a reticular distance $d = 2.64$ Å corresponding to fresnoite. This small crystal is supported by a second crystal, which is expected to be a BT grain in view of both the size and the reticular distance ($d = 2.09$ Å).

temperature higher than 1200°C in standard conditions does not allow attaining 90% of density while the full transformation of the initial amorphous silica into fresnoite is already obtained. The crystallization into fresnoite disrupts the continuity of the silica dielectric phase separating the BT grains. The structural matching between fresnoite and BT, confirmed by HRTEM, suggests that the composite is no longer formed by two distinct phases as in classical ferroelectric/dielectric composites.

Crystallization is governed by two kinetic steps, nucleation and growth. The increase of the heating rate from low temperature, where the nucleation rate of the crystals is fast, can delay the onset of crystallization.[35,36] In the same way, reducing the sintering time would help limiting fresnoite growth. For this purpose, advanced sintering techniques such as SPS and μ-wave sintering were used to densify BT500–Si5 particles. Both techniques provide extremely high heating rates enhancing the consolidation rate of powders. In the case of SPS, the combination of pressure and electric current activates and enhances densification. In particular, pressure can help densification by overcoming the restraining stress at the interface. The extremely accelerated kinetics should prevent excessive nucleation at low temperature and lead to more complete densification before extensive crystallization. In addition, short sintering times (3 min for SPS and 5 for μ-wave) and quenching conditions in both SPS and μ-wave techniques favor the freezing of the high-temperature microstructure.

The sample, sintered 3 min at 1050°C by SPS under Argon atmosphere, exhibits a peculiar microstructure made of rounded grains with a melted looking aspect (Fig. 9(a)). Uncoated BT grains sintered in exactly similar SPS sintering conditions are shown for sake of comparison. The density of the ceramic reaches 82% instead of 70% when using standard sintering at a similar temperature during 2 h. Slightly increasing the sintering temperature significantly raises the density up to more than 90% but with unavoidable reduction phenomena leading to a strong conductivity contribution. Dielectric experiments show a reduction and a flattening of the maximum of losses at T_c compared with the ceramic made of uncoated grains sintered in the same SPS conditions (Fig. 9(b)). This proves that the silica shell is preserved in the final composite, as confirmed by HRTEM observations. The existence of an amorphous phase in the vicinity of the grain boundaries has been pointed out in thin slices, obtained using ultramicrotomy, of SPS ceramics (Fig. 10(a)). The micrograph is representative of several zones on the sample. Small fresnoite crystals were also observed (Fig. 10(b)). More generally, an enlarged view of the slice confirms that BT grains are not interpenetrating.

Microwave sintering performed at a temperature estimated to be close to 1200°C leads to higher density of 92%. The reproducibility of these experiments was checked and confirmed. In addition, because we used a susceptor, microwave sintering is no longer considered as a volumic sintering and the microstructure remains homogeneous, as confirmed by HRSEM imaging. No blisters occur and grain growth is still avoided whereas the final sintering stage here is attained (Fig. 9(a)). Dielectric measurements can be once more used as an intrinsic probe to check the efficiency of the silica loss barrier. The loss values still remain stable and well below 1%, while the permittivity reaches 3000 at room temperature (Fig. 9(b)).

IV. Conclusion

Silica-coated ferroelectric particles were investigated with, as a front edge challenge, the control of the interfaces in such bulk nanostructured composites. The first step was to perform an accurate and deep investigation of the complex silica/ferroelectric interface. Postmortem and *in situ* TEM experiments showed the presence of amorphous silica up to 1000°C. Neck formation with an associated redistribution of silica around the ferroelectric core was observed below 850°C. Fresnoite crystallites appeared in the temperature range 850°–1000°C in agreement with both XRD and dilatometric investigations. Postmortem chemical probing at the nanoscale strongly supports a diffusion process from the BT core, i.e. Ba diffusion into the silica shell. Electron diffraction investigation of the interface showed that the fresnoite cluster growth at the BT surface is chemically and structurally favored. Creation of a dislocation network is believed to help in relaxing the lattice mismatch. In addition, a partial coverage of the ferroelectric core by fresnoite particles was confirmed by XPS probing. Such a high level of interface probing was never reported in such silica-nanostructured ceramics. The second step was to process nanostructured ceramic composites using advanced sintering processes such as SPS and microwave sintering. In both cases, the permittivity attained at least 2000 at room temperature and a stabilization of the dielectric losses, well below 1%, was obtained with, in particular, a significant flattening of the losses at the Curie temperature, thus signing the preservation of the core–shell architecture. This

was supported by HRTEM observation on a thin SPS ceramic slice obtained by ultramicrotomy.

The possible structural and chemical matching between BT and fresnoite, and the close correspondence evidenced between XPS spectra of BT/SiO_2 thin films and ceramics made of $BT@SiO_2$ particles, open routes to process multifunctional composites with multilayer design.

Acknowledgments

We thank Dominique Denux for TMA and Eric Lebraud for XRD measurements.

References

[1]F. Caruso, "Nanoengineering of Particle Surfaces," *Adv. Mater.*, **13**, 11–22 (2001).

[2]R. Davies, G. A. Schurr, P. Meenan, R. D. Nelson, H. E. Bergna, C. A. S. Brevett, and R. H. Goldbaum, "Engineered Particle Surfaces," *Adv. Mater.*, **10**, 1264–70 (1998).

[3]G. J. de A. A. Soller-Illia, C. Sanchez, B. Lebeau, and J. Patarin, "Chemical Strategies to Design Textured Materials: From Microporous and Mesoporous Oxides to Nanonetworks and Hierarchical Structures," *Chem. Rev.*, **102**, 4093–133 (2002).

[4]F. Garcia Santamaria, V. Salgueiriño-Maceira, C. Lopez, and L. M. Liz-Marzan, "Synthetic Opals Based on Silica-Coated Gold Nanoparticles," *Langmuir*, **18**, 4519–22 (2002).

[5]F. Grasset, N. Labhsertwar, D. Li, D. C. Park, N. Saito, H. Haneda, O. Cador, T. Roisnel, S. Mornet, E. Duguet, J. Portier, and J. Etourneau, "Synthesis and Magnetic Characterization of Zinc Ferrite Nanoparticles with Different Environments: Powder, Colloidal Solution, and Zinc Ferrite–Silica Core–Shell Nanoparticles," *Langmuir*, **18**, 8209–16 (2002).

[6]C. R. Vestal and Z. J. Zhang, "Synthesis and Magnetic Characterization of Mn and Co Spinel Ferrite-Silica Nanoparticles with Tunable Magnetic Core," *Nanoletters*, **3**, 1739–43 (2003).

[7]L. M. Liz-Marzán and P. Mulvaney, "The Assembly of Coated Nanocrystals," *J. Phys. Chem. B*, **107**, 7312–26 (2003).

[8]M. T. Buscaglia, V. Buscaglia, and R. Alessio, "Coating of $BaCO_3$ Crystals with TiO_2: Versatile Approach to the Synthesis of $BaTiO_3$ Tetragonal Nanoparticles," *Chem. Mater.*, **19**, 711–8 (2007).

[9]S. Mornet, C. Elissalde, V. Hornebecq, O. Bidault, E. Duguet, A. Brisson, and M. Maglione, "Controlled Growth of Silica Shell on $Ba_{0.6}Sr_{0.4}TiO_3$ Nanoparticles Used as Precursors of Ferroelectric Composites," *Chem. Mater.*, **17**, 4530–6 (2005).

[10]J. Y. Lee, J.-H. Lee, S.-H. Hong, Y. K. Lee, and J.-Y. Choi, "Coating $BaTiO_3$ Nanolayers on Spherical Ni Powders for Multilayer Ceramic Capacitors," *Adv. Mater.*, **15**, 1655–8 (2003).

[11]M. D. Sacks, N. Bozkurt, and G. W. Scheiffele, "Fabrication of Mulitte-Matrix Composites by Transient Viscous Sintering of Composite Powders," *J. Am. Ceram. Soc.*, **74**, 2428–37 (1991).

[12]H. Giesche and E. Matijevic, "Preparation, Characterization, and Sinterability of Well-Defined Silica/Yttria Powders," *J. Mater. Res.*, **9**, 436–49 (1994).

[13]H. Y. Tian, J. Q. Qi, Y. Wang, J. Wang, H. L. W. Chan, and C. L. Choy, "Core-Shell Structure of Nanoscaled $Ba_{0.5}Sr_{0.5}TiO_3$ Self-Wrapped by MgO Derived from a Direct Solution Synthesis at Room Temperature," *Nanotechnology*, **16**, 47–52 (2005).

[14]L. F. Hakim, D. M. King, Y. Zhou, C. J. Gump, S. George, and A. W. Weimer, "Nanoparticle Coating for Advanced Optical, Mechanical and Rheological Properties," *Adv. Funct. Mater.*, **17**, 3175–81 (2007).

[15]R. Chen, A. Cui, X. Wang, Z. Gui, and L. Li, "Structure, Sintering Behavior and Dielectric Properties of Silica-Coated $BaTiO_3$," *Mater. Lett.*, **54**, 314–7 (2002).

[16]J. S. Park and Y. H. Han, "Nano Size $BaTiO_3$ Powder Coated with Silica," *Ceram. Int.*, **31**, 777–82 (2005).

[17]H. P. Abicht, D. Völzke, and H. Schmidt, "Preparation, Characterization and Sintering Behavior of Barium Titanate Powders Coated with Ba-, Ca-, Si- and Ti-Containing Components," *Mater. Chem. Phys.*, **51**, 35–41 (1997).

[18]D. Völzke and H. P. Abicht, "The Influence of Different Additives and The mode of their Addition on the Sintering Behaviour and the Properties of Semiconducting Barium Titanate Ceramics," *Solid State Sci.*, **2**, 149–59 (2000).

[19]M. C. Foster, D. J. Arbogast, R. M. Nielson, P. Photinos, and S. C. Abrahams, "Fresnoite: A New Ferroelectric Mineral," *J. Appl. Phys.*, **85**, 2299–303 (1999).

[20]A. Halliyal, A. S. Bhalla, S. A. Markgraf, L. E. Cross, and R. E. Newnham, "Unusual Pyroelectric and Piezoelectric Properties of Fresnoite ($Ba_2TiSi_2O_8$) Single Crystal and Polar Glass-Ceramics," *Ferroelectrics*, **62**, 27–38 (1985).

[21]K.-H. Felgner, T. Müller, H. T. Langhammer, and H-P. Abitch, "Investigations on the Liquid Phase in Barium Titanate Ceramics with Silica Additives," *J. Eur. Ceram. Soc*, **21**, 1657–60 (2001).

[22]J. Muños Saldaña, B. Mullier, and G. A. Schneider, "Preparation of $BaTiO_3$ Single Crystals Using the Modified SiO_2-Exaggerated Grain Growth Method," *J. Eur. Ceram. Soc.*, **22**, 681–8 (2002).

[23]S. Mornet, C. Elissalde, O. Bidault, F. Weill, E. Sellier, O. Nguyen, and M. Maglione, "Ferroelectric-Based Nanocomposites: Towards Multifunctional Materials," *Chem. Mater.*, **19**, 987–92 (2007).

[24]U.-C. Chung, C. Elissalde, S. Mornet, M. Maglione, and C. Estournès, "Controlling Internal Barrier in Low Loss $BaTiO_3$ Supercapacitors," *Appl. Phys. Lett.*, **94**, 0729031–3 (2009).

[25]S. Marinel and G. Desgardin, "A New Inductive Furnace Based on Microwave Irradiation for Growing Long $YBa_2Cu_3O_{7-\delta}$ Single-Domain Bars," *Adv. Mater.*, **17** [10] 1448–52 (1998).

[26]M. D. Sacks and T. Y. Tseng, "Preparation of SiO_2 Glass from Model Powder Compacts: II, Sintering," *J. Am. Ceram. Soc*, **67**, 532–7 (1984).

[27]A. J. Jagota, "Simulation of the Viscous Sintering of Coated Particles," *J. Am. Ceram. Soc.*, **77**, 2237–9 (1994).

[28]L. T. Zhuravlev, "The Surface Chemistry of Amorphous Silica. Zhuravlev Model," *Colloids Surf A*, **173**, 1–38 (2000).

[29]M. D. Sacks and T. Y. Tseng, "Preparation of SiO_2 Glass from Model Powder Compacts: I, Formation and Characterization of Powders, Suspensions, and Green Compacts," *J. Am. Ceram. Soc.*, **67**, 526–31 (1984).

[30]Z.-C. Chen, T. A. Ring, and J. Lemaître, "Stabilization and Processing of Aqueous $BaTiO_3$ Suspension with Polyacrylic Acid," *J. Am. Ceram. Soc.*, **75**, 3201–8 (1992).

[31]W.-H. Shih, D. Kisailus, and Y. Wei, "Silica Coating on Barium Titanate Particles," *Mater. Lett.*, **24**, 13–5 (1995).

[32]D. A. Anderson, J. H. Adair, D. Miller, J. V. Biggers, and T. R. Shrout, "Surface Chemistry Effects on Ceramic Processing of $BaTiO_3$ Powders"; pp. 485–92 in *Ceramic Transactions. Ceramic Powder Science II*, Vol. 1, Edited by G. L. Messing, E. R. Fuller, and H. Hausner. American Ceramic Society, Columbus, OH, 1988.

[33]Y. Gao, Y. Masuda, and K. Koumoto, "Microstructure-Controlled Deposition of $SrTiO_3$ Thin Film on Self-Assembled Monolayers in an Aqueous Solution of $(NH_4)_2TiF_6Sr(NO_3)_2H_3BO_3$," *Chem. Mater.*, **15**, 2399–410 (2003).

[34]J. Majimel, D. Bacinello, E. Durand, F. Vallée, and M. Tréguer-Delapierre, "Synthesis of Hybrid Gold-Gold Sulfide Colloidal Particles," *Langmuir*, **24**, 4289–94 (2008).

[35]P. C. Panda, W. M. Mobley, and R. Raj, "Effect of the Heating Rate on the Relative rates of Sintering and Crystallization in Glass," *J. Am. Ceram. Soc.*, **72**, 2361–4 (1989).

[36]J. L. Keddie and E. P. Giannelis, "Effect of Heating Rintering of Titanium Dioxide Thin Films: Competition Between Densification and Crystallization," *J. Am. Ceram. Soc.*, **74**, 2669–71 (1991). □